Mon. Not. R. Astron. Soc. **000**, 1–18 (1999) Printed 31 March 2000 (MN LATEX style file v1.4)

Hydroxyl lines towards Puppis A

Beate Woermann[1,2⋆], Michael J. Gaylard[1] and Robina Otrupcek[3]
[1] *Hartebeesthoek Radio Astronomy Observatory, PO Box 443, Krugersdorp 1740, South Africa*
[2] *Department of Physics & Electronics, Rhodes University, Grahamstown 6140, South Africa*
[3] *Australia Telescope National Facility, PO Box 76, Epping, NSW 2121, Australia*

Accepted 2000. Received 2000 ; in original form 2000

ABSTRACT
The 1667 MHz ground-state hydroxyl (OH) line has been observed towards positions on Puppis A as well as in the immediate vicinity of this supernova remnant (SNR). The spectra at two positions on Puppis A show absorption lines at velocities less than +7.6 km s^{-1}, and emission lines above this velocity. Analysis of all four 18 cm OH lines indicates that Puppis A must lie between the OH clouds seen in absorption and emission, giving it a v_{lsr} of +7.6 km s^{-1}. This implies that the kinematic distance to Puppis A is $1.3^{+0.6}_{-0.8}$ kpc.

The OH clouds in front of Puppis A are slightly anomalously excited, as shown by analysis of the four 18 cm OH lines at the two observed positions on Puppis A. There is no evidence of any interaction of the SNR with the clouds in front of and behind it.

Key words: ISM: individual: Puppis A – ISM: molecular clouds OH – ISM: supernova remnants

1 INTRODUCTION

Reliable distance estimates to supernova remnants (SNRs) are desirable for studies of intrinsic properties such as explosion energy, for statistical studies of the properties of SNRs at all wavelengths and the relationship of SNRs to the interstellar medium. Distances to SNRs are usually inferred from the distances to HI and HII regions, molecular clouds, OB associations and pulsars that are considered to be associated with the SNR. Distances can also be deduced from the optical velocities and proper motions of filaments, as well as x-ray observations of the remnants. All of these methods have been used in the past to determine a distance to the Puppis A SNR, and they are reviewed below.

Kinematic distances derived from the velocity of an associated cloud depend on the galactic rotation model used. The models used prior to 1986 are generally based on a galactocentric distance (R_0) of 10 kpc. Hence the kinematic distances to Puppis A based on the velocity of an associated object determined prior to ∼1986 should be scaled by 0.85 for a valid comparison with more recent results. Such scaled distances have been included, where appropriate, in parentheses after the distance quoted in the literature.

The discovery of fast-moving oxygen filaments in Puppis A by Winkler & Kirshner (1985) led to the determination of the distance to this SNR from the proper motion of these filaments over time by Dechristopher & Winkler (1994). They combined the expansion proper motions and radial velocities of such filaments from an 8 yr baseline to obtain a kinematic distance of 1.9 kpc to Puppis A.

Sakhibov & Smirnov (1983) and Huang & Thaddeus (1985) both assumed that Puppis A is associated with or gave rise to the Vela OB1 Association (G265.0 − 1.0), which has a spectrophotometric distance of 1.8 kpc as determined by Humphreys (1978). Sakhibov & Smirnov (1983) also used the radial velocity of this OB Association to obtain a kinematic distance of 2.2 ± 1.0 (1.9 ± 0.85) kpc to it and Puppis A.

Gosachinskij & Khersonskij (1985) identified an HI envelope around Puppis A from data with a velocity resolution of 6.3 km s^{-1}. The velocity centre of this HI hole is at +5 km s^{-1}. While the authors translated this into a kinematic distance of 2 kpc (using $R_0 = 10$ kpc), the flat rotation curve of Fich, Stark & Blitz (1989) gives a distance of 0.9 kpc.

Detailed scenarios of the interaction of Puppis A and molecular clouds have been proposed (Dubner & Arnal 1988, Arendt et al. 1990, Reynoso et al. 1995). Based on earlier publications, Dubner & Arnal (1988) assumed the distance to Puppis A to be 2.0 ± 0.3 kpc. Adopting a flat rotation curve and $R_0 = 8.5$ kpc, material at this distance would have $v_{lsr} = +14.5 \pm 2.5$ km s^{-1}, giving an estimate of the systemic velocity for Puppis A. Using HI and CO observations, Dubner & Arnal (1988) showed that there is a molecular cloud to the east of the remnant at $v_{lsr} = +16$ km s^{-1}, in agreement with the assumed systemic velocity of the SNR. The interlocking shapes of the cloud at +16 km s^{-1} and the shockfront of the SNR were interpreted as evidence for the present expansion of the SNR into this cloud (see Fig.2 in

⋆ E-mail: beate@bootes.hartrao.ac.za

Dubner & Arnal 1988). Further work based on this scenario is reported in Reynoso et al. (1995), entrenching the kinematic distance of 2.2 kpc to Puppis A. Reynoso et al. (1995) proposed that clouds referred to as Feature A at $v_{lsr} = +3.6$ km s^{-1} and B at $v_{lsr} = +19.2$ km s^{-1} define the radial velocity limits of the expanding molecular envelope around Puppis A and thus derive an approximate expansion velocity of 8±5 km s^{-1} for the remnant.

Zarnecki et al. (1978) determined a distance of only 1 kpc from the absorbing-column density of cold matter derived from the best fit to the continuum x-ray spectrum. Szymkowiak (1985) obtained 2.5 kpc in similar manner from more recent x-ray data. These extremes of 1 kpc and 2.5 kpc for the distance to Puppis A, determined by the same method but based on different measurements, highlight the difficulties involved in obtaining accurate distances to SNRs.

Other distance estimates to Puppis A are based on proposed radio surface brightness-to-diameter ($\Sigma - D$) relationships. Thus, using their versions of the $\Sigma - D$ relationship, Milne (1971), Downes (1971) and Clark & Caswell (1976) determined distances of 1.2, 2.2 and 2.5 kpc respectively to Puppis A. Milne, Goss & Danziger (1983), comparing two different versions of this relationship, obtained 1.8 kpc and 2.4 kpc according to the $\Sigma - D$ relationships of Milne (1979) and Caswell & Lerche (1979) respectively. The latter value cannot be considered a separate distance determination as Puppis A (assumed to be at 2.4 kpc) is one of the 33 sources used by Caswell & Lerche to calibrate their $\Sigma - D$ relationship. Huang & Thaddeus (1985) also used Puppis A as one of the calibrators of their $\Sigma - D$ relationship.

Green (1984, 1991) has questioned the usefulness of the $\Sigma - D$ relationship, based on the unreliability of the distance determinations to the calibrators. Furthermore, it has been shown for middle-aged SNRs in M33 (Gordon et al. 1999), which are all effectively at the same distance from us, that the intrinsic properties of SNRs vary significantly. Yet the $\Sigma - D$ relationship is based on the assumption that there is a unique relationship between the linear diameters of SNRs and their radio surface brightness. Nevertheless attempts to obtain a satisfying $\Sigma - D$ relationship persist. The most recent version for Galactic supernova remnants was produced by Case & Bhattacharya (1998). Again Puppis A is included in the calibrator list, this time using the distance of 2.2 kpc derived by Reynoso et al. (1995).

The widely used distance of 2.2 kpc derived from the apparent association with the +16 km s^{-1} east cloud (Reynoso et al. 1995) can be tested by using molecular lines that are sensitive to the background radio continuum brightness temperature (T_{bg}). The ground state lines of hydroxyl (OH) are suitable for this as the excitation temperatures (T_{ex}) of the 1665 and 1667 MHz transitions are typically 5 – 8 K (Crutcher 1979). Whether the lines appear in emission or absorption depends strongly on the brightness temperature of the material behind the OH emitting cloud, along the line of sight. In brief, if $T_{ex} > T_{bg}$, the line is seen in emission; if $T_{ex} < T_{bg}$ the line is seen in absorption, assuming $\tau > 0$.

In the case of Puppis A a number of molecular clouds are known to lie along the line of sight through the SNR. If some lie in front of the SNR and some behind, the transition from absorption in foreground clouds which have the bright SNR behind them, to emission from clouds behind the SNR, which have a lower T_{bg}, marks the v_{lsr} (radial velocity) at which the SNR lies, permitting a kinematic distance determination using a galactic rotation curve. The OH method of distance determination is not absolute as it relies on rotation curves to get kinematic distances, but it can show clearly which molecular clouds are in front and which are behind the SNR given suitable values of T_{ex} and T_{bg}.

The OH observations towards Puppis A are described in section 2 and the results in section 3.1. All four ground-state OH lines were observed and detected towards two positions on Puppis A. Thus the excitation temperatures of the four OH lines for the absorbing clouds could be determined as shown in section 3.3. The constraints derived from the OH spectra for the distance to Puppis A are given in section 4. The implications of this new distance for previously derived parameters of this SNR are discussed in section 5.

2 OBSERVATIONS

Observations were made in the frequency switching mode with the 18 cm system of the 26-m antenna at the Hartebeesthoek Radio Observatory (HartRAO), South Africa and the 20-cm system of the 22-m Mopra antenna near Coonabarabran, NSW, Australia.

The observations at HartRAO were made in one polarization only i.e. left-hand circularly polarized (LCP). Initial spectra were obtained in 1993. A velocity resolution of 1.1 km s^{-1} was used. The observed spectrum at the centre position of Puppis A showed unresolved lines. Thus observations on it were repeated at a velocity resolution of 0.54 km s^{-1} in 1999. The average zenith system temperature of the HartRAO system was 45 K and its point source sensitivity was 10 JyK^{-1} as measured on Hydra A. The beamwidth of the antenna is 30′.

The 20 cm receiver system at Mopra provided simultaneous left- and right-hand circular polarizations. The average zenith system temperature was 34 K at 1665 MHz for both polarizations. The point source sensitivity was 12.7 Jy K^{-1}, as measured on Virgo A (A. Tzioumis, private communication). At 1665 MHz the half power beamwidth of the Mopra antenna is 33′. The observations at Mopra were made in 1994 March. The spectra obtained at Mopra have a velocity resolution of 0.84 km s^{-1}.

The observations include positions chosen to sample the material in the area surrounding Puppis A, such as the east cloud (Dubner & Arnal 1988, Reynoso et al. 1995) and the Reflection nebula R1 (Herbst 1975).

3 RESULTS

3.1 The 1667 MHz spectra towards positions P1 to P11

The Hanning smoothed OH 1667 MHz spectra, labeled P1 to P11, are shown at the observed positions superimposed on a contour map of the radio brightness temperature of Puppis A and surroundings from the 2326 MHz Rhodes/HartRAO continuum survey (Jonas, Baart & Nicolson 1998) in Fig.1. Table 1 lists the OH 1667 MHz line parameters of the unsmoothed spectra as well as the velocity ranges over which emission or absorption features are visible.

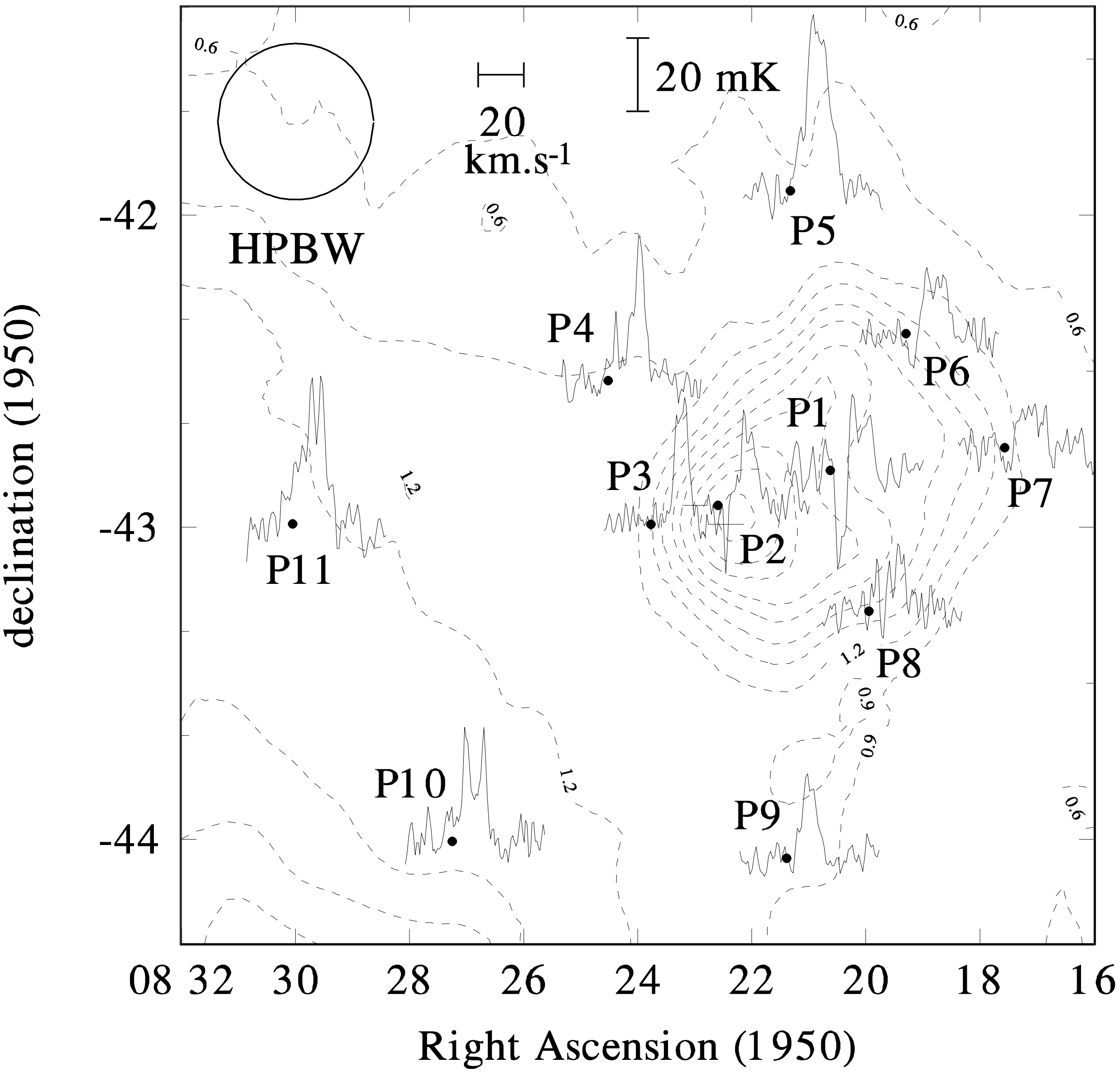

Figure 1. The Hanning-smoothed 1667 MHz OH spectra are shown superimposed on the 0.33° resolution Rhodes University/HartRAO 2326 MHz brightness temperature map (Jonas, Baart & Nicolson 1998). All unmarked contours are higher than those labelled, and in order of increasing T_b are 1.6, 2.0, 2.5, 2.9, 3.5, 4.0 and 4.7 K. The solid circles show the observed positions. The spectra are oriented so that 0 km s^{-1} v_{lsr} is at the dot marking the observed position. The hollow circle represents the approximate halfpower beamwidth of the antennas at 18cm. Scalebars for the line antenna temperature and velocity are also given.

Inspection of Figs. 1 and 2 and column 5 in Table 1 shows that there are three main components in the spectra. The highest velocity component ranges from +8 to +20 km s^{-1} and is always present in emission. The unsmoothed 1667 MHz spectra (see Figs. 2 – 5) show that this component may be due to several clouds at different velocities, whose emission has blended into a roughly gaussian shape. The lowest velocity component is present in the range 0 to +4.5 km s^{-1}. This component is present at P1, P2 and P4 as a narrow line ($\Delta v \leq 2.2$ km s^{-1}) with the line velocity in the four OH lines varying from +3.2 to +3.8 km s^{-1}. We thus refer to this component with the label +3.5 km s^{-1}. In some positions it is present in emission, in others in absorption. The absorption component at +6.7 km s^{-1} is present only at one position, P1. At some positions off Puppis A the low and high velocity components have merged into a single broad emission line. The spectra clearly sample the clouds and features listed in Table 1 of Reynoso et al. (1995). A discussion of the individual spectra follows.

Position P1: (see Fig. 3.) This is at the approximate cen-

Table 1. The position labels, coordinates, spectral resolution, and velocity ranges of observed OH 1667 MHz emission and absorption lines towards Puppis A. The line antenna temperatures, T_A, velocities, v_{lsr}, and widths, Δv, were obtained from multiple gaussian fits to the spectra. Absorption lines are present where the line antenna temperature is negative.

1 Position label	2 Equ coords (B1950)	3 Galactic coords	4 resolution [km.s^{-1}]	5 vel. range [km.s^{-1}]	6 T_A [mK]	7 v_{lsr} [km.s^{-1}]	8 Δv [km.s^{-1}]
P1	$08^h20^m38'$, $-42°49'$	G260.40 − 3.40	0.54	+2 to +4	−35 ± 6	3.6 ± 0.3	2.2 ± 0.7
			0.54	+6 to +7.5	−39 ± 11	6.7 ± 0.3	1.7 ± 0.5
			0.54	+8 to +10.5	+12 ± 6	8.1 ± 1.0	2.5 ± 1.2
			0.54	+12 to +17	+17 ± 4	14.6 ± 0.6	5.3 ± 2.2
P2	$08^h22^m36^s$, $-42°56'$	G260.70 − 3.17	0.84	+2.5 to +4.5	−24 ± 7	3.5 ± 0.2	0.9 ± 0.3
			0.84	+8 to +19	+20 ± 3	13.2 ± 0.6	8.0 ± 1.5
P3	$08^h23^m46^s$, $-42°59'$	G260.88 − 3.03	0.84	+10 to +18	+33 ± 3	13.6 ± 0.3	6.6 ± 0.7
P4	$08^h24^m31^s$, $-42°32'$	G260.58 − 2.65	0.84	+2.5 to +4.5	+24 ± 7	3.5 ± 0.2	0.9 ± 0.4
			0.84	+8.5 to +19	+33 ± 3	13.5 ± 0.3	6.2 ± 0.8
P5	$08^h21^m19^s$, $-41°55'$	G259.74 − 2.78	1.10	+1 to +22	+44 ± 3	11.9 ± 0.4	11.3 ± 0.9
P6	$08^h19^m17^s$, $-42°23'$	G259.90 − 3.35	0.84	+1 to +4.5	−13 ± 5	3.1 ± 0.6	4.6 ± 1.7
			0.84	+6 to +20.5	+15 ± 2	12.0 ± 1.5	12.5 ± 2.8
P7	$08^h17^m34^s$, $-42°45'$	G260.02 − 3.82	0.84	−0.5 to +4	∼ −5		
			0.84	+4 to +19	+11 ± 2	11.5 ± 1.1	9.9 ± 2.0
P8	$08^h19^m58^s$, $-42°16'$	G260.70 − 3.76	0.84	+0.5 to +4.5	< +12		
			0.84	+8 to +16.5	+14 ± 4	13.1 ± 0.9	6.6 ± 2.4
P9	$08^h21^m23^s$ $-44°04$	G261.50 − 4.0	1.10	+4 to +16.5	+21 ± 4	9.8 ± 0.6	6.8 ± 1.3
P10	$08^h27^m15^s$ $-44°00'$	G262.07 − 3.11	0.84	+4.5 to +16	+26 ± 6	6.5 ± 0.5	4.8 ± 1.7
					+27 ± 6	13.7 ± 0.4	3.1 ± 1.2
P11	$08^h30^m03^s$ $-42°59'$	G261.55 − 2.10	1.10	−5.0 to +19.5	+31 ± 4	9.0 ± 0.8	12.8 ± 2.1

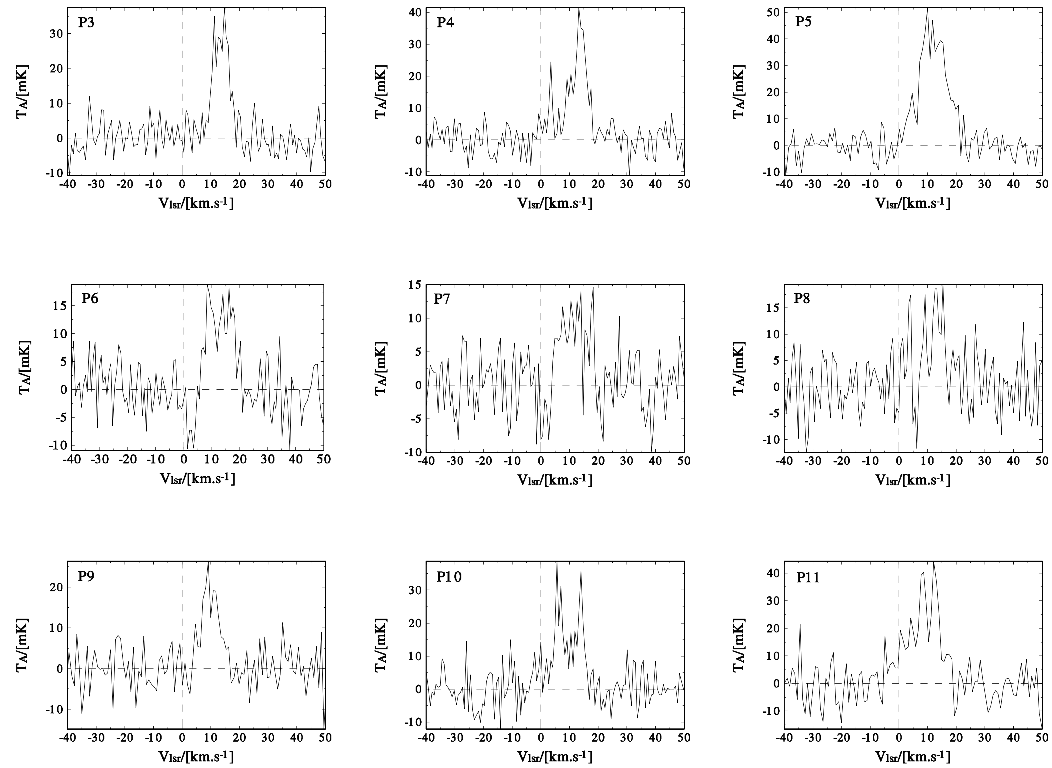

Figure 2. The unsmoothed 1667 MHz OH spectra at positions P3 – P11 are shown.

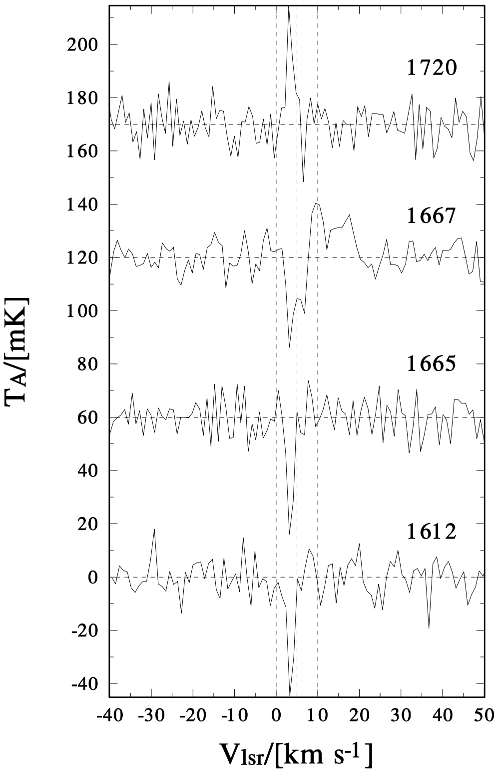

Figure 3. The four ground state OH lines at position P1, on the centre of Puppis A, at a resolution of 1.1 km s^{-1}

.

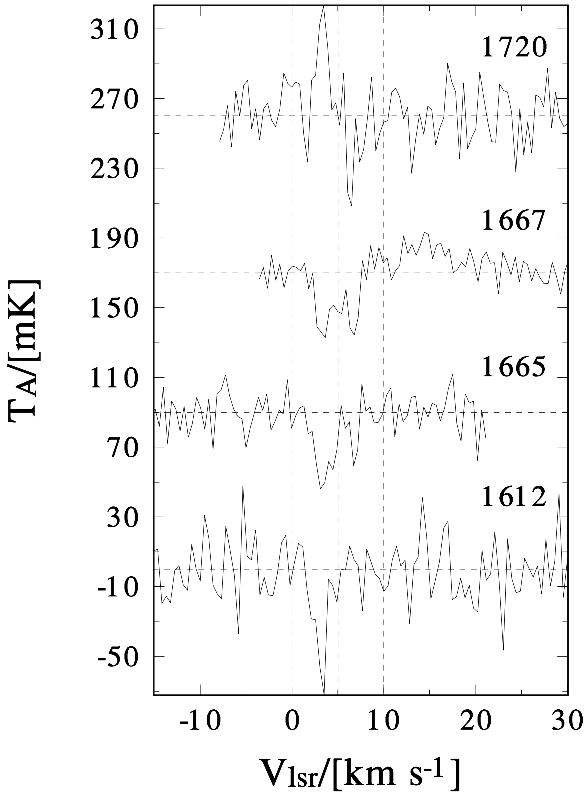

Figure 4. The four ground state OH lines at position P1, on the centre of Puppis A, at a resolution of 0.54 km s^{-1}.

tre of Puppis A. As the absorption component in the 1667 MHz spectrum at a resolution of 1.1 km s^{-1} could be interpreted as two lines, we reobserved all four lines at twice the resolution. These are shown in Fig. 4, where two absorption components are visible at both 1667 and 1665 MHz. At 1667 there are also two emission components at higher velocities. The two absorption components at +3.5 km s^{-1} (Feature A in Table 1 of Reynoso et al. 1995) and +6.7 km s^{-1} must lie in front of Puppis A, which provides a background radiation temperature higher than the excitation temperature of the OH (see section 3.3). The two OH 1667 MHz components at +8.5 km s^{-1} (Northern Cloud in Table 1 of Reynoso at al. 1995) and +16 km s^{-1} (East Cloud in Reynoso et al. 1995) are seen in emission and must lie beyond Puppis A. The zero-crossing velocity from absorption to emission is +7.6 km s^{-1}. The implications of this spectrum for the distance to Puppis A are discussed in section 4.

The component at +6.7 km s^{-1} has not been reported previously. However, this is not surprising as the VLA HI observations of Reynoso et al. (1995) have a velocity resolution of only 5.2 km s^{-1}. The earlier work of Dubner & Arnal (1988) has a velocity resolution of 2.1 km s^{-1} in the HI observations and 0.26 km s^{-1} in the CO observations. The latter observations did not fully sample the region that fills the beam of $\sim 30'$ at this position in the 1667 MHz OH line. Thus the region responsible for the 6.7 km s^{-1} absorption line must have a small angular extent compared to that of Puppis A.

Position P2: (see Fig. 5.) This is approximately on the radio peak of Puppis A, which is off-centre. Here only one low velocity absorption line, at +3.5 km s^{-1} (Feature A), is detected followed by a higher velocity emission line at +13.2 km s^{-1} (eastern cloud and others at +14 km s^{-1} in Table 1 of Reynoso et al. 1995). At this position little, if anything, of the northern cloud at +8 km s^{-1} lies in the beam. Thus the transition from the absorption to the emission line is not as abrupt as on the centre position P1. This spectrum confirms that Puppis A is situated in front of the clouds at +14 km s^{-1} and behind the +3.5 km s^{-1} cloud.

Position P3: (see Fig. 2.) This is on the edge of the CO east cloud, just outside Puppis A. Thus roughly half the beam is filled by the CO east cloud and the other half by Puppis A. The absence of a line at +3.5 km s^{-1} may thus be explained by the presence of roughly equally strong lines, one in absorption due to Puppis A and another in emission as in the +3.5 km s^{-1} component in the spectrum at P4. The emission detected at this position covers the same velocity range as the emission in positions P1 and P2 and is in close agreement with the velocity of +16 km s^{-1} quoted for the CO and HI observations on the east cloud by Dubner & Arnal (1988) and Reynoso et al. (1995). Together with the high velocity emission seen at position P1 and P2 this indicates that the CO east cloud extends well into the region behind Puppis A.

Position P4: (see Fig. 2.) This is on the centre of the CO east cloud as shown in Arendt, Dwek & Petre (1991)

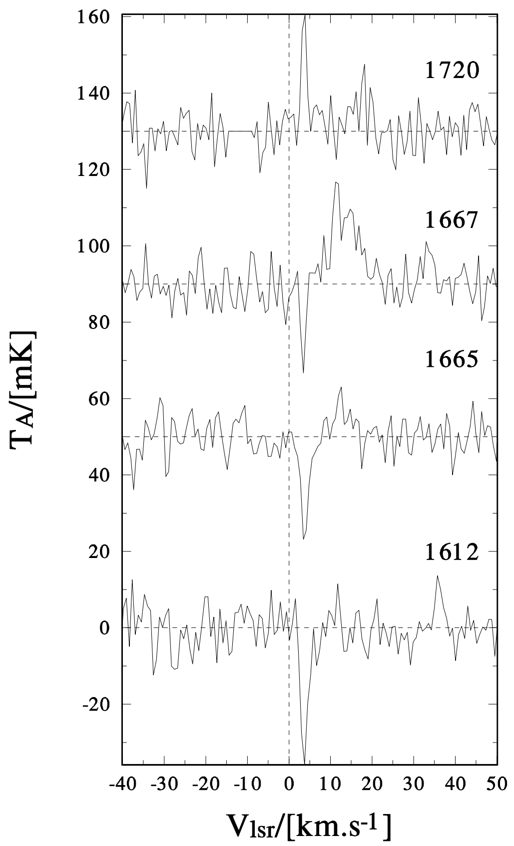

Figure 5. The four ground state OH lines at position P2, on the radio peak of Puppis A, at a resolution of 0.84 km s^{-1}.

and does not include Puppis A in the beam at all. No absorption feature is seen. However emission is present at a velocity of +3.5 km s^{-1}, i.e. that of the lower velocity absorption line detected at positions P1 and P2. The higher velocity emission occurs between +8.5 and +19 km s^{-1}, indicating that some of the features at +8 and +14 km s^{-1} listed in Table 1 of Reynoso et al. (1995) are present, as well as the east cloud at +14 to +19 km s^{-1}. The emission line features seen here and at positions P1, P2 and P3 do not change dramatically in intensity from the positions on Puppis A to this one, which is clearly off Puppis A. Thus the emission at velocities greater than +8 km s^{-1} must be from clouds situated beyond Puppis A. An example of the marked change in line intensity due to a significant change in background temperature is that observed in the +3.5 km s^{-1} line seen at P1, P2 and P4.

Position P5: (see Fig. 2.) This is towards the reflection nebula Puppis R1. It shows relatively strong emission between +1 and +22 km s^{-1}. This position is well outside the angular extent of Puppis A.

Positions P6: (see Fig. 2.) Puppis A lies partially in the beam at this position (Fig. 1) and absorption is present at 0 to +4 km s^{-1}. This absorption is not as strong as at P1 and P2. As much of the northern cloud at +8 km s^{-1} lies in the beam at this position, its emission is fairly strong in this spectrum and thus the transition from the absorption feature to the high velocity emission is abrupt.

Position P7: (see Fig. 2.) Puppis A fills less than half the beam at this position. Nevertheless there is weak evidence for the 0 to +4 km s^{-1} absorption feature seen at other positions on Puppis A. Emission is seen over the same velocity range as at the other positions.

Position P8: (see Fig. 2.) The OH at this position is very faint, but the same emission features as seen at other positions on the edge of Puppis A appear to be present. At this position the +3.5 km s^{-1} feature, if present, is in emission and the +6.7 km s^{-1} feature is in absorption.

Positions P9, P10 and P11: (see Fig. 2) These are in the region around Puppis A and at least 1 beam width away from its edge. These positions show the same velocity components as seen at the positions on and very close to Puppis A, indicating that the molecular clouds are fairly extended. All the OH is seen in emission only.

3.2 The four OH lines towards positions P1 and P2

In order to investigate the excitation temperatures of the OH clouds in the direction of Puppis A all four ground state hydroxyl lines were observed at positions P1 and P2. The resultant spectra are shown in Figs. 3 (1.1 km s^{-1} resolution), 4 (0.54 km s^{-1} resolution) and 5 (0.84 km s^{-1} resolution). The line parameters obtained by fitting multiple gaussian profiles are listed in Tables 2, 3 and 4.

3.3 Excitation temperatures and optical depths in the OH clouds towards Puppis A

Transitions between the four lowest energy levels of OH, all belonging to the $^2\Pi_{3/2}$, J=3/2 ground state, give rise to radio lines at approximately 1612, 1665, 1667 and 1720 MHz. Let the subscripts 1, 2, 3 and 4 refer to the 1612, 1665, 1667 and 1720 MHz OH lines respectively, such that ν_1 and $T_{ex,1}$ are the frequency and excitation temperature of the 1612 MHz line respectively etc. These four lines, i = 1..4, obey the following nine equations (Rogers & Barrett 1967 and Goss 1968)

$$\frac{\nu_1}{T_{ex,1}} + \frac{\nu_4}{T_{ex,4}} = \frac{\nu_2}{T_{ex,2}} + \frac{\nu_3}{T_{ex,3}} \tag{1}$$

$$T_{A,i} = \eta_B \, F \, (T_{ex,i} - T_{bg}) \, \tau_i \tag{2}$$

$$N(OH) = C_i \, T_{ex,i} \, \tau_i \, \Delta v_i \tag{3}$$

where $T_{A,i}$ is the line antenna temperature, T_{bg} is the brightness temperature of the background continuum at 18cm, η_B the beam efficiency, τ_i is the optical depth and F is the beam filling factor. The latter has a value of one if the OH cloud fills the antenna beam. For clouds of angular size smaller than the antenna beam F is less than one. N_{OH} is the OH column density in cm^{-2} and Δv_i is the full width at half maximum of the optical depth profile i.e the line width in km s^{-1}. C_1 to C_4 are equal to 22.21, 4.299, 2.385 and 20.84 in units of 10^{14} cm^{-2} K^{-1} (km $s^{-1})^{-1}$ respectively (Goss, 1968). In thermal equilibrium the intensities of the four lines are in the ratio 1:5:9:1 respectively.

If all four OH lines have been observed at a position, then $T_{A,i}$, η_B and Δv_i are known for each line. T_{bg} has to be found independently. That leaves four line excitation temperatures, four line optical depths, the OH column density

Table 2. The line parameters of gaussian fits to the four ground-state OH spectra obtained at Position P1 with a velocity resolution of 1.1 km s^{-1}.

freq/[MHz]	T_A/[mK]	v_{lsr}/[km s^{-1}]	Δv/[km s^{-1}]
1720	$+45 \pm 13$	3.3 ± 0.2	1.1 ± 0.6
1667	-34 ± 7	3.4 ± 0.2	1.2 ± 0.5
	-29 ± 21	6.6 ± 0.5	2.7 ± 1.3
	$+25 \pm 8$	9.1 ± 1.1	4.0 ± 3.0
	$+15 \pm 4$	16.3 ± 1.0	4.7 ± 1.8
1665	-48 ± 11	3.4 ± 0.2	1.2 ± 0.4
1612	-47 ± 11	3.5 ± 0.2	1.1 ± 0.5

Table 3. The line parameters of gaussian fits to the four ground-state OH spectra obtained at Position P1 with a velocity resolution of 0.54 km s^{-1}.

freq/[MHz]	T_A/[mK]	v_{lsr}/[km s^{-1}]	Δv/[km s^{-1}]
1720	$+63 \pm 16$	3.3 ± 1.2	1.1 ± 0.4
	-65 ± 15	6.3 ± 0.1	0.3 ± 0.2
1667	-35 ± 6	3.6 ± 0.3	2.2 ± 0.7
	-39 ± 11	6.7 ± 0.3	1.7 ± 0.5
	$+12 \pm 6$	8.1 ± 1.0	2.5 ± 1.2
	$+17 \pm 4$	14.6 ± 0.6	5.3 ± 2.2
1665	-42 ± 8	3.5 ± 0.2	2.2 ± 0.5
	-35 ± 10	6.8 ± 0.1	0.3 ± 0.2
1612	-63 ± 24	3.2 ± 0.2	1.3 ± 0.8

Table 4. The line parameters of gaussian fits to the four ground-state OH spectra obtained at Position P2 with a velocity resolution of 0.84 km s^{-1}.

freq/[MHz]	T_A/[mK]	v_{lsr}/[km s^{-1}]	Δv/[km s^{-1}]
1720	$+34 \pm 8$	3.6 ± 0.1	1.0 ± 0.3
1667	-24 ± 7	3.5 ± 0.2	0.9 ± 0.3
	$+20 \pm 3$	13.2 ± 0.6	8.0 ± 1.5
1665	-27 ± 6	3.8 ± 0.2	2.0 ± 0.6
	$+9 \pm 4$	12.6 ± 1.0	4.4 ± 2.5
1612	-34 ± 9	3.8 ± 0.3	1.5 ± 0.6

Table 5. OH cloud parameters for the +13 km s^{-1} line at position P2.

F	$N(OH)$ /[cm^{-2}]	$T_{ex,1}$ /[K]	$T_{ex,2}$ /[K]	$T_{ex,3}$ /[K]	$T_{ex,4}$ /[K]	τ_1	τ_2	τ_3	τ_4
0.7	1.75	6.5	6.5	6.5	6.5	0.0020	0.0104	0.0188	0.0022

Table 6. OH cloud parameters for the +3.5 km s^{-1} lines at positions P1 and P2.

position	F	$N(OH)$ /[cm^{-2}]	$T_{ex,1}$ /[K]	$T_{ex,2}$ /[K]	$T_{ex,3}$ /[K]	$T_{ex,4}$ /[K]	τ_1	τ_2	τ_3	τ_4
P1	0.5	1.82	1.26	5.0	6.5	-2.5	0.036	0.047	0.065	-0.019
P2	0.5	0.63	1.26	5.0	6.5	-2.5	0.019	0.024	0.034	-0.010

Table 7. OH cloud parameters for the +6.7 kms^{-1} line at position P1.

F	$N(OH)$ /[cm^{-2}]	$T_{ex,1}$ /[K]	$T_{ex,2}$ /[K]	$T_{ex,3}$ /[K]	$T_{ex,4}$ /[K]	τ_1	τ_2	τ_3	τ_4
0.3 to 0.4	0.4	-6.5	$+5.0$	$+6.0$	$+2.0$	-0.010	$+0.05$	$+0.07$	$+0.03$

and the filling factor as unknowns—a total of 10 unknowns. If the nine equations are solved for different assumed values of the filling factor, the solutions for the other nine unknowns may be chosen as those giving the smallest errors overall in the resultant $N(OH)$, $T_{ex,i}$ and τ_i. We used the method of Newton-Raphson iteration to obtain our solutions.

We estimated the background temperatures, T_{bg}, on and off Puppis A, from the 2326 MHz Rhodes University/HartRAO southern sky survey (Jonas, Baart & Nicolson 1998), smoothed to a resolution of 0.5°. The 13 cm values were converted to 18 cm values using the radio spectral indicies of the components. Puppis A has a spectral index of 2.5 (Green 1971). We used a spectral index of 2.65 for the galactic background estimated from a minimum in the map at the galactic latitude of Puppis A. Including the contribution from the cosmic microwave background this gave background temperatures of 3.4 K, 9.4 K and 8.5 K for the clouds behind Puppis A, at P2 in front of Puppis A and at P1 in front of Puppis A respectively.

Before considering the full solutions to the equations for positions P1 and P2, the 1667 MHz line excitation temperature of the clouds emitting the +3.5 km s^{-1} line can be estimated independently using the on-source (at P1 and P2) and off-source (at P4) line intensities. If we assume that T_{ex}, τ and F do not change from the on-source to the off-source positions then equation 2 can be solved for the excitation temperature using the on-source and off-source line parameters and background temperatures. For position P1 and P4 this gives an excitation temperature of 5.5 K, which is similar to the value of 6.4 K obtained for position P2 and P4.

As all the lines detected here are fairly faint, small deviations from thermal equilibrium can be masked by the uncertainties in the subtracted baselines and the line strengths. Thus at position P2 the line seen in emission at +13 km s^{-1} is greater than the noise in the spectra only at 1665 and 1667 MHz. It thus appears to be close to thermal equilibrium with an excitation temperature in the range 5 to 8 K (Crutcher 1979) for filling factors in the range 0.4 to 0.9. We adopt 6.5 K for T_{ex} and 0.7 for F as representative of the solutions obtained (see Table 5) from the nine equations above assuming thermal equilibrium. A background temperature of 3.4 K was used, as the cloud emitting this line is positioned behind Puppis A. Reasonable solutions are obtained where the main lines are in equilibrium with a T_{ex} of 6.5 K and T_{ex} in the range 4 to 19 K for the 1612 MHz and 1720 MHz lines. A main-line anomaly may exist with a difference in the main line T_{ex} of up to about 4 K.

Using the line parameters and antenna parameters given in Tables 3 and 4, the excitation temperatures, OH column densities and optical depths given in Tables 6 and 7 were derived using Equations 1 – 3.

The subtle effects of a small main line anomaly are far more readily observed where a high background temperature amplifies them. Thus at P1 the main lines at +3.5 km s^{-1} cannot be in thermal equilibrium as the 1665 MHz line is deeper than the 1667 MHz line, rather than being in the thermal ratio of 5:9. The strong 1720 MHz line is due to a negative excitation temperature and optical depth, and is amplifying the strong background radiation source.

From an inspection of the HI high angular resolution images in Figs. 2 and 5 of Reynoso et al. (1995), the +3.5 km s^{-1} HI emission feature covers the area towards and around Puppis A in a patchy fashion. This leads us to an estimate of the filling factor in the range 0.3 - 0.6.

At position P1 the minimum in the solution space for the physical parameters of the cloud emitting the +3.5 km s^{-1} line is fairly well defined, whereas at position P2 the solution space is flatter. Nevertheless the different values do not range too widely. As at both positions the minimum occurs near a solution giving the same excitation temperature in the four lines at the two positions, we chose that solution (see Table 6) as representative of the cloud parameters. The 6.5 K excitation temperature for the 1667 MHz line in this solution is similar to the values of 5.5 K and 6.4 K obtained above for the on-source and off-source calculations of the excitation temperature.

As the +6.7 km s^{-1} line at position P1 is not properly resolved, even at a resolution of 0.54 km s^{-1}, no solution is obtained from Equations 1 to 3 with the uncertainties in the line parameters given in Table 3. By doubling the uncertainties in the line strengths, a reasonable approach given that the lines are unresolved, we obtained the solutions listed in Table 7. The values indicate that the cloud emitting this line is, as expected from the line parameters, optically thin and not very extended (i.e. low filling factor).

Although it cannot be ruled out that Puppis A is expanding into either of the clouds in front of it (at +3.5 km s^{-1} and +6.7 km s^{-1}) or immediately behind it (+8.1 km s^{-1}), there is no specific evidence in these spectra for such an interaction. The minor deviations from thermal equilibrium of the four lines shown here are quite common in the interstellar medium (Crutcher, 1979). Because we have been able to solve the equations 1 – 3 for all four lines at +3.5 km s^{-1}, it is clear that the 1720 MHz emission lines at P1 and P2 are seen because there is a bright background source, i.e. Puppis A. They are not due to the superficially similar 1720 MHz maser emission that can occur in supernova remnants interacting with molecular clouds (Frail et al. 1996 and references therein).

4 DISTANCE TO PUPPIS A

In the light of the evidence presented above we place Puppis A between the adjacent absorbing (+6.7 km s^{-1}) and emitting (+8.1 km s^{-1}) cloud velocities. We adopt the zero crossing velocity as the systemic velocity of Puppis A. This is +7.6 ± 0.5 km s^{-1} where the uncertainty is taken to be the velocity resolution of the spectrum.

Conversion of this velocity to a distance is dependent on the assumption that the absorbing and emitting clouds have no peculiar motion as well as on the particular Galactic rotation curve used. We use the flat rotation curve of Fich et al. (1989) with a galactocentric distance of 8.5 kpc and Ω_o = 220 km s^{-1}. The latter gives practically identical distance values to those given by the linear fit rotation curve of Fich et al. (1989), provided that the correct Ω_o, i.e. 221.641 km s^{-1} as given in their Equation 23, is used for the linear fit. We thus obtain a distance of 1.30 ± 0.08 kpc to the SNR. If the line velocities of the lines on either side of the transition from absorption to emission are considered as the limits on the distance, then we have $+7.6^{+0.5}_{-0.9}$ km s^{-1}, giving a distance of $1.3^{+0.07}_{-0.13}$ kpc to the remnant.

As noted above, this assumes that the clouds do not have any peculiar velocity relative to the galactic rotation velocity. The average peculiar velocity of such dark clouds is generally thought to be 5 km s^{-1} (Brand & Blitz 1993 and references therein). If this is taken as the error in the systemic velocity of the SNR we have $+7.6\pm5$ km s^{-1}, giving a distance of $1.3^{+0.6}_{-0.8}$ kpc.

5 DISCUSSION AND CONCLUSION

The limits of the systemic velocity of Puppis A given by the adjacent absorption and emission 1667 MHz OH lines at P1 clearly do not give an expansion velocity for the neutral envelope around the young Puppis A SNR. As there is no evidence in the spectra for an interaction of these clouds with the SNR, these clouds may well be some distance away from Puppis A along our line of sight. The emission from the neutral envelope, if it exists, thus blends with that of other material along the line of sight. Given that we detect no further lines than those listed in Tables 1 – 4 out to ±50 km s^{-1} we have no evidence for a neutral shell around Puppis A in the observations reported here.

It is interesting that the systemic velocity for Puppis A of $+5$ km s^{-1} reported by Gosachinskij & Khersonskij (1985) is in close agreement with that of $+7.6$ km s^{-1} reported here. Nevertheless, the clearly defined HI envelope in Fig. A12 of Gosachinskij & Khersonskij (1985) giving an expansion velocity of 8 km s^{-1} has not been reported elsewhere.

Previously the interlocking shapes of the CO/HI east cloud at $+16$ km s^{-1} and the eastern shockfront of the SNR were interpreted as evidence for the present expansion of the SNR into this cloud (see Fig. 2 in Dubner & Arnal 1988; Reynoso et al. 1995). This was believed to be further supported by the presence of a bright x-ray emission knot in the east of the remnant (Petre et al. 1982). This eastern x-ray knot is attributed to the shock front overrunning a dense external cloud (Teske & Petre 1987, Blair et al. 1995, Arendt et al. 1990). As the morphology of the shell in radio and x-ray maps in this region points to a retardation of the shock front, Petre et al. (1982) claim that the shock front has not yet completely engulfed the cloud as the shock front has not yet reconnected beyond it.

The OH observations presented above cannot be reconciled with the idea that the SNR expanding into the east molecular cloud at $+16$ km s^{-1}, as the SNR clearly lies in front of the OH at $+8.1$ km s^{-1}. There is thus no convincing observational evidence for a cloud that is responsible for retarding the shock front at the x-ray east knot. We suggest that the shock front has for all practical purposes completely engulfed the external molecular cloud giving rise to the x-ray knot, thus leaving no observable unshocked remainder of the cloud. In support of this point of view we note that Blair et al. (1995) point out that their FUV spectrum of the x-ray east knot leaves little doubt that the entire cloud has been enveloped by the blast wave.

The 1720 MHz emission line at a velocity of $+3.5$ km s^{-1} detected at positions P1 and P2 does not have the characteristics associated with molecular clouds interacting with SNRs (Frail et al. 1996). Nevertheless it is puzzling that Frail et al. (1996) did not detect this line with the Parkes telescope in their search for 1720 MHz masers towards SNRs, given the sensitivity of their observations. The 1667 MHz OH absorption lines reported here at positions on Puppis A are of the type used by Green (1989) to obtain contraints on distances to SNRs.

This revised distance to Puppis A gives more support to the identification of a cooling neutron star near the centre of this SNR. With the previous distance estimate of 2.2 kpc this stellar remnant would have had to have travelled at 1000 km s^{-1} to reach its present position $6'$ to the northwest of the expansion centre (Petre, Becker & Winkler 1996). At a distance of 1.3 kpc this velocity is effectively halved, putting it more in line with a recent estimate of the mean pulsar space velocity of 450 ± 90 km s^{-1} (Lyne & Lorrimer, 1994).

With the distance reduced to 1.3 kpc the angular diameter of $\sim 50'$ of Puppis A (Green 1971) implies a physical diameter of only ~ 20 pc.

REFERENCES

Arendt R.G., Dwek E., Petre R., 1991, ApJ, 368, 474
Arendt R.G., Dwek E., Petre R., Dickel J.R., Roger R.S., Milne D.K., Kesteven M.J., 1990, ApJ, 350, 266
Blair W.P., Raymond J.C., Long K.S., Kriss G.A., 1995, ApJ, 454, L35
Brand J., Blitz L., 1993, A&A, 275, 67
Case G.L., Bhattacharya D., 1998, ApJ, 504, 761
Clark D.H., Caswell J.L., 1976, MNRAS, 174, 267
Caswell J.L., Lerche I., 1979, MNRAS, 187, 201
Crutcher R.M., 1979, ApJ, 234, 881
Dechristopher B.M., Winkler P.F., 1994, BAAS, 26, 951
Downes D., 1971, AJ, 76, 305
Dubner G.M., Arnal E.M., 1988, A&AS, 75, 363
Fich M., Blitz L., Stark A.A., 1989, ApJ, 342, 272
Frail D.A., Goss W.M., Reynoso E.M., Giacani E.B., Green A.J., Otrupcek R., 1996, AJ, 111, 1651
Gordon S.M., Duric N., Kirshner R.P., Goss W.M., Viallefond F., 1999, ApJS, 120, 247
Gosachinskij I.V., Khersonskij V.K., 1985, Ap&SS, 108, 303
Goss W.M., 1968, ApJS, 15, 131
Green A.J., 1971, AJP, 24, 773
Green D.A., 1984, MNRAS, 209, 449
Green D.A., 1989, MNRAS, 238, 737
Green D.A., 1991, PASP, 103, 209
Herbst W., 1975, AJ, 80, 212
Huang Y.-L., Thaddeus P., 1985, ApJ, 295, L13
Humphreys R.M., 1978, ApJS, 38,309
Jonas J.L., Baart E.E., Nicolson G.D., 1998, MNRAS, 297, 977
Lyne A.G., Lorrimer D.R., 1994, Nature, 369, 127
Milne D.K., 1971, AJP, 24, 429
Milne D.K., 1979, AJP, 32, 83
Milne D.K., Goss W.M., Danziger I.J., 1983, MNRAS, 204, 237
Petre R., Canizares C.R., Kriss G.A., Winkler P.F., 1982, ApJ, 258, 22
Petre R., Becker C.M., Winkler P.F., 1996, ApJ, 465, L43
Reynoso E.M., Dubner G.M., Goss W.M., Arnal E.M., 1995, AJ, 110, 318
Rogers A.E.E, Barrett A.H., 1967, in van Woerden H., ed, Radio Astronomy and the Galactic System, North-Holland Publishing Co.
Sakhibov F.Kh., Smirnov M.A., 1983, SvA, 27(4), 395
Szymkowiak A.E., 1985, PhD thesis, University of Maryland
Teske R.G., Petre R., 1987, ApJ, 314, 673
Winkler P.F., Kirshner R.P., 1985, ApJ, 299, 981
Zarnecki J.C., Culhane J.L., Toor A., Seward F.D., Charles P.A., 1978, ApJ, 219, L17